CHEMISTRY
A EUROPEAN JOURNAL

DOI: 10.1002/chem.201100899

Multifunctional Manganese Carbonate Microspheres with Superparamagnetic and Fluorescent Properties: Synthesis and Biological Application

Juan Peng,[a] Li-Na Feng,[a] Kui Zhang,[b] Jing-Jing Li,[a] Li-Ping Jiang,*[a] and Jun-Jie Zhu*[a]

Abstract: Multifunctional manganese carbonate microspheres with superparamagnetic and fluorescent properties were fabricated and used as biological labels. The Fe_3O_4@$MnCO_3$ microspheres were synthesized by direct coprecipitation without any linker shell. The Fe_3O_4@$MnCO_3$ microspheres have uniform size distribution and rough surface, which provides a promising template for the assembly of polyelectrolytes (PEs) and CdTe quantum dots (QDs). A luminescent CdTe shell was observed in Fe_3O_4@$MnCO_3$@PE-CdTe spheres by confocal fluorescence imaging. With excellent solubility in water and rough surfaces, the multifunctional microsphere offers a friendly microenvironment for immobilization of α-fetoprotein (AFP) antibodies (Ab_2) to fabricate Fe_3O_4@$MnCO_3$@PE-CdTe-Ab_2 architecture. By using the Fe_3O_4@$MnCO_3$@PEs-CdTe-Ab_2 bioconjugate as a label, a promising and versatile platform for fluorescence imaging and electrochemical immunosensing of cancer biomarker AFP was developed. The prepared electrochemical immunosensor shows high sensitivity and selectivity with a detection limit of 0.3 pg mL^{-1}.

Keywords: α-fetoprotein · fluorescent probes · immunoassays · magnetic properties · manganese carbonate

Introduction

Recently, there has been remarkable progress in the synthesis of nanomaterials and their exploitation for various applications.[1,2] Superparamagnetic Fe_3O_4 nanoparticles have been intensively studied and applied in bioseparation,[3] drug targeting,[4] cell isolation,[5] enzyme immobilization,[6] catalysis,[7] and wastewater treatment.[8] Quantum dots (QDs) have also attracted great attention ever since their first milestone application as luminescent labels in biological detection.[9] Due to their interesting optical and electronic properties, QDs are widely used today as versatile materials in biosensing[10–12] and diagnostics.[13–15] When QDs are conjugated with biomolecules like proteins, which have fascinating macromolecular structure in terms of their unique recognition, transport, and catalytic properties, not only can they act as alternative labels to molecular fluorophores as fluorescence biological probes, but they also can be functionalized in electrochemical biosensors or bioassays.[16–20] However, due to their small size, these QD–protein bioconjugates are inclined to aggregate, which greatly limits their applications.[21]

In addition, a new trend in materials science has emerged in the last years, focused on the development of multifunctional materials by incorporation of both magnetic and fluorescent nanoparticles into single entity.[22–24] So far, considerable efforts have been made in the design of silica containing both Fe_3O_4 nanoparticles and QDs.[25,26] The fabrication methods include the use of magnetic particles and QDs as cores followed by growth of a silica shell[26] and the inverse suspension method.[27] More recently, magnetic and fluorescent silica spheres have been prepared by using silica-coated magnetic nanoparticles as cores, followed by the assembly of QDs at the core surface.[22] However, the smooth surface of silica spheres restricts the loading of QDs to a monolayer, which limits their application in bioassays. Therefore, a good host is of paramount importance for incorporation of Fe_3O_4 nanoparticles and QDs for subsequent applications.

Manganese carbonate has been intensively investigated owing to its abundance in nature and applications in lithium batteries,[28,29] catalysis,[30] water treatment,[31] and solid precursors for metal oxide synthesis.[32,33] Spherical $MnCO_3$ is of particular interest because of its biocompatibility, surface porous structure, and low specific gravity. $MnCO_3$ microspheres have been employed as templates for fabrication of

[a] J. Peng, L.-N. Feng, J.-J. Li, Dr. L.-P. Jiang, Prof. J.-J. Zhu
State Key Lab of Analytical Chemistry for Life Science
School of Chemistry and Chemical Engineering
Nanjing University, Nanjing 210093 (P. R. China)
Fax: (+86) 2-583-597-204
E-mail: Jianglp@nju.edu.cn
jjzhu@nju.edu.cn

[b] Prof. K. Zhang
The Affiliated Drum Tower Hospital of
Nanjing University Medical School
Nanjing, 210008 (P. R. China)

Supporting information for this article is available on the WWW under http://dx.doi.org/10.1002/chem.201100899.

WILEY ONLINE LIBRARY
© 2011 Wiley-VCH Verlag GmbH & Co. KGaA, Weinheim

various kinds of microcapsules,[34,35] as they can be decomposed under mild conditions of dissolution. These characteristics have led to $MnCO_3$ microspheres being used in drug delivery,[36,37] protein encapsulation,[38,39] biosensing,[40,41] and antimicrobial agents.[42] Compared to silica spheres, $MnCO_3$ microspheres also have the advantage of easier preparation, low cost, and good dispersibility in water. However, the large size of $MnCO_3$ microspheres (>3 μm) limits their applications in bioassays. Thus, a facile way to prepare $MnCO_3$ spheres smaller than 1 μm is a great challenge and highly desirable.

Here we report the synthesis of multifunctional $MnCO_3$ microspheres with superparamagnetic and fluorescent properties (Scheme 1a). Superparamagnetic Fe_3O_4@$MnCO_3$ microspheres with a diameter of about 600 nm were synthesized by one-step co-precipitation in glycerol/water. The rough surface of the Fe_3O_4@$MnCO_3$ microspheres offers a promising template for assembly of PEs and QDs to fabricate Fe_3O_4@$MnCO_3$@PEs-CdTe microspheres. The multifunctional microspheres have uniform size distribution, good solubility, and dispersibility in water, and are thus suitable for immobilization of α-fetoprotein antibodies (Ab_2) to fabricate Fe_3O_4@$MnCO_3$@PEs-CdTe-Ab_2 architectures. By using the bioconjugates as labels, a versatile platform for fluorescence imaging and electrochemical detection of cancer biomarker α-fetoprotein (AFP) is thus developed (Scheme 1b). Notably, this technique can be easily adapted for loading other types of QDs to obtain desired optical and electrochemical labels for multiplexed assay and diagnostic applications.

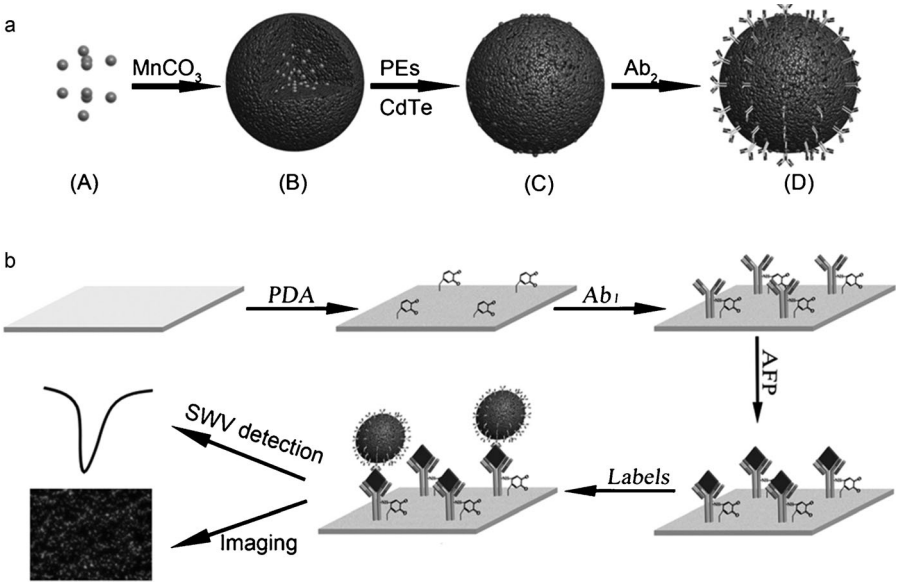

Scheme 1. a) Schematic illustration of the fabrication process of Fe_3O_4@$MnCO_3$@PEs-CdTe-Ab_2 3D architecture. A) Fe_3O_4 nanoparticle. B) Fe_3O_4@$MnCO_3$ microsphere. C) Fe_3O_4@$MnCO_3$@PEs-CdTe microsphere. D) Fe_3O_4@$MnCO_3$@PEs-CdTe-Ab_2 bioconjugate. b) Principle of immunosensor for fluorescence imaging and electrochemical detection of AFP based on Fe_3O_4@$MnCO_3$@PEs -CdTe-Ab_2 labels.

Results and Discussion

Characterization of multifunctional $MnCO_3$ microspheres: Fe_3O_4@$MnCO_3$ microspheres were synthesized by a co-precipitation reaction in glycerol/water. Fe_3O_4 nanoparticles with the size of around 8 nm were synthesized with good monodispersity according to reference [43] (see Figure S1 in the Supporting Information). Because the Fe_3O_4 nanoparticles strongly interact with Mn^{2+} in solvent, no primer is required to promote deposition and adhesion of the $MnCO_3$ layer. Figure 1A shows an SEM image of the Fe_3O_4@$MnCO_3$ microspheres. The as-prepared Fe_3O_4@$MnCO_3$ microspheres have uniform structure and rather rough surface. Figure 1B shows a high-resolution TEM image of the Fe_3O_4@$MnCO_3$ microspheres. The Fe_3O_4 nanoparticles are entrapped in the $MnCO_3$ microspheres because of aggregation of the Fe_3O_4 nanoparticles prior to or during the coating process. The Fe_3O_4@$MnCO_3$ microspheres have an average diameter of about 600 nm (Figure 1C). The surface of the microsphere is rough, in agreement with the SEM image. The unique structure of the Fe_3O_4@$MnCO_3$ microspheres with a high surface area of 27.21 $m^2 g^{-1}$ makes them very attractive for material-loading purposes.

The magnetic properties of the Fe_3O_4@$MnCO_3$ microspheres were recorded with a SQUID magnetometer (Figure 2A). The field-dependent magnetization curve exhibits no hysteresis at 300 K, demonstrating the superparamagnetic characteristics of the Fe_3O_4@$MnCO_3$ microspheres. The saturation magnetization of the superparamagnetic Fe_3O_4@$MnCO_3$ microspheres is approximately 50.0 emu g^{-1}, which is lower than the saturation magnetization of the Fe_3O_4 nanoparticles of 70.0 emu g^{-1}.[43] This could be explained by taking into account the thick $MnCO_3$ shell surrounding the magnetic cores. Figure 2B shows photographs of the suspension of Fe_3O_4@$MnCO_3$ in the absence and in the presence of an external magnet. The particles can be easily dispersed in water to form a brown suspension and be drawn from the solution to the sidewall of the vial by an external magnetic field. The magnetic particles can be brought again back into the original solution by removing the external field and then slightly agitating. These magnetic properties can allow the microspheres to be used in bioseparation and bioassay since they

 © 2011 Wiley-VCH Verlag GmbH & Co. KGaA, Weinheim

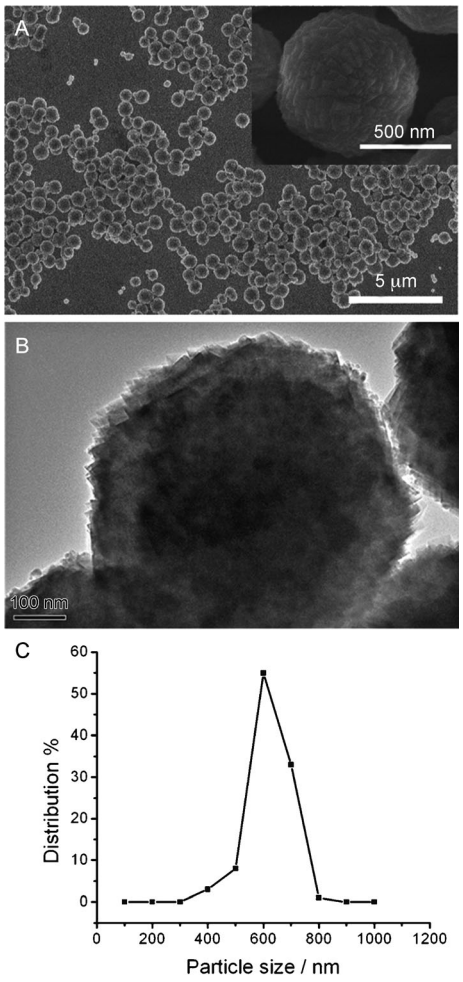

Figure 1. A) SEM image of Fe_3O_4@$MnCO_3$ microspheres. Inset: higher magnification image of Fe_3O_4@$MnCO_3$ microspheres. B) HRTEM image of Fe_3O_4@$MnCO_3$ microspheres. C) Size distribution of Fe_3O_4@$MnCO_3$ microspheres.

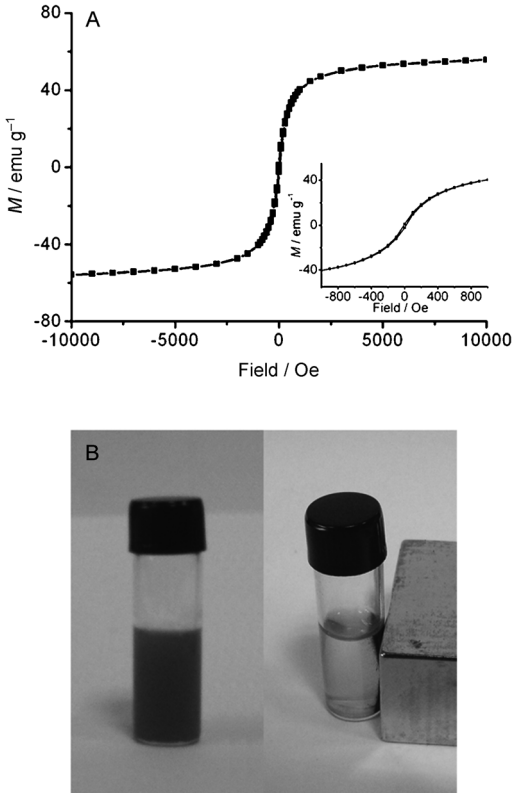

Figure 2. A) Magnetization curve of the Fe_3O_4@$MnCO_3$ microspheres at 300 K. Inset: zoomed area of the magnetization curve at low magnetic field. B) Photographs of a solution of Fe_3O_4@$MnCO_3$ microspheres in the absence and presence of a external magnet.

undergo strong magnetization, allowing for efficient magnetic separation under an applied external magnetic field.

CdTe QDs were deposited on Fe_3O_4@$MnCO_3$ microspheres by using an electrostatic layer-by-layer method. A PE film consisting of poly(sodium 4-styrenesulfonate) (PSS) and poly(allylamine hydrochloride) (PAH) thin layers was applied to the Fe_3O_4@$MnCO_3$ microspheres. The layer-by-layer assembly process was monitored by ζ-potential measurement, which is an effective method for characterization of the surface charge of microspheres.[43] Figure S2 in the Supporting Information shows the ζ-potentials of Fe_3O_4@$MnCO_3$, Fe_3O_4@$MnCO_3$/PSS, Fe_3O_4@$MnCO_3$/PSS/PAH, and Fe_3O_4@$MnCO_3$@PEs-CdTe microspheres, and of Fe_3O_4@$MnCO_3$@PEs-CdTe-Ab_2 bioconjugate. The Fe_3O_4@$MnCO_3$ microspheres are positively charged at neutral pH with a potential of +8.9 mV, which could be explained by an excess of manganese(II) cations. The carbonate ion reacts with additional H^+, whereas manganese remains absorbed on the particle surface. Subsequent alternating absorption of PSS and PAH layers onto the surface yielded potentials of −23.7 and +21.0 mV, respectively. The positively charged Fe_3O_4@$MnCO_3$@PEs microspheres could be further used in the loading of CdTe QDs. The ζ-potential of Fe_3O_4@$MnCO_3$@PEs-CdTe was −28.0 mV. The larger shift and more negative value of the potential after the loading process results from a larger adsorbed amount of CdTe QDs on the outer surface.

The deposition process of CdTe QDs onto the microspheres was also monitored by fluorescence (see Figure S3 in the Supporting Information). Compared to the Fe_3O_4@$MnCO_3$ microspheres, a strong emission at 531 nm was observed for the Fe_3O_4@$MnCO_3$@PEs-CdTe microspheres, indicating effective deposition of CdTe QDs onto the microspheres. After the assembly of CdTe QDs, the maxima of the emission spectrum is blueshifted compared to the original CdTe QDs. Carboxyl-capped CdTe QDs show higher photostability in the presence of an excess of free carboxyl stabilizer. However, in this case, the carboxyl group can interact with cationic groups ($-NH^{3+}$) of the PAH layer to produce unprotected CdTe QDs on the surface of the microspheres, which could explain the spectral shifts toward shorter wavelengths.[22] The inset in Figure S3 in the Supporting Information shows the fluorescence spectra of the as-prepared CdTe QDs and the supernatant after adsorption of CdTe QDs on Fe_3O_4@$MnCO_3$ microspheres. The obvious decrease in the intensity of the emission peak

 © 2011 Wiley-VCH Verlag GmbH & Co. KGaA, Weinheim

at 544 nm indicates adsorption of CdTe QDs onto the microspheres.

The loading of CdTe QDs on the microspheres can be calculated by the difference in intensity of the emission peak at 544 nm of the initial CdTe QD solution before and after loading.[44] A rough estimate indicated that 1.0 mg of Fe_3O_4@$MnCO_3$@PEs microspheres could accommodate 6.3×10^{14} CdTe QDs. In a control experiment, Fe_3O_4@$MnCO_3$ microspheres without PE coating were loaded with CdTe QDs, and the loading was 2.1×10^{14} CdTe QDs for 1 mg of Fe_3O_4@$MnCO_3$ microspheres. These results indicate that the polyelectrolyte layers are very important for loading of the CdTe QDs. First, the polyelectrolyte layers could increase the loading of CdTe QDs. With PAH as the outmost layer on the microspheres, the CdTe loading was thrice that on the Fe_3O_4@$MnCO_3$ microspheres alone. The cationic groups ($-NH^{3+}$) of the positively charged PAH interact so strongly with the negatively charged carboxylate ($-COO^-$) groups on the surface of the CdTe QDs[21] that the loading is greatly increased when PE layers are involved. Meanwhile, since the positively charged PAH also introduced more positive charge onto the surface of the Fe_3O_4@$MnCO_3$ microspheres, the enhanced electrostatic interaction between the QDs and the microspheres also contributes to the increased loading. The second role of the polyelectrolyte layers lies in the inhibition of fluorescence quenching after loading of CdTe QDs. Compared to Fe_3O_4@$MnCO_3$@PEs microspheres, the fluorescence of the microspheres without PEs layers decreases rapidly. This result could be ascribed to the fact that the PE layers increase the distance between the microspheres and the CdTe QDs. In addition, the PE layers also prevented aggregation of the Fe_3O_4@$MnCO_3$ microspheres by introducing more positive charges onto the microspheres.

Confocal laser-scanning fluorescence microscopy was also used to demonstrate the distribution of the CdTe QDs in the Fe_3O_4@$MnCO_3$ microspheres (Figure 3). The CdTe QDs are uniformly distributed in the microspheres. Due to highly effective loading of QDs, an obvious fluorescent CdTe shell is observed for the CdTe-loaded microspheres.

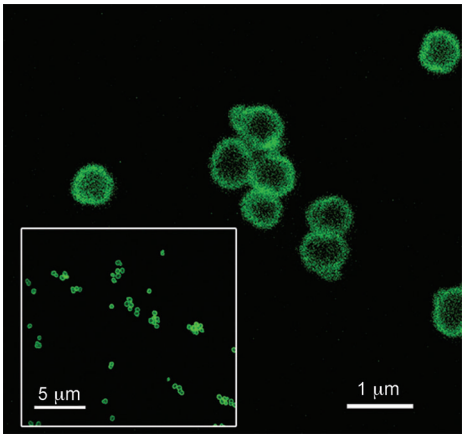

Figure 3. Confocal fluorescence images of Fe_3O_4@$MnCO_3$@PEs-CdTe microspheres. Inset: overview of the microspheres

Assembly of Ab_2 on Fe_3O_4@$MnCO_3$@PEs-CdTe microspheres: Fe_3O_4@$MnCO_3$@PEs-CdTe can inherit the advantages of its parent materials, such as good solubility and dispersity in water. Ab_2 can be conjugated to Fe_3O_4@$MnCO_3$@PEs-CdTe through strong interactions between the amino group of the protein and the carboxylic group of the CdTe surface. As shown in Figure 4, the bioconjugates show strong absorbance around 280 nm (peak a) for the protein, and weak absorbance at 523 nm (peak b) for CdTe. The fluorescence intensity decreased after loading of the protein (Figure S3, Supporting Information). With an isoelectric point of pH 7.4, AFP antibodies are positively charged at pH 7.0 in PBS, and could be easily assembled onto Fe_3O_4@$MnCO_3$@PEs-CdTe microspheres via electrostatic interaction. The potential of the microspheres changed from −28.0 to −5.7 mV after binding with Ab_2 (Figure S2, Supporting Information). This result also confirms that Ab_2 could be effectively linked to the surface of Fe_3O_4@$MnCO_3$@PEs-CdTe microspheres, while avoiding protein cross-linking and retaining their specific immunorecognition ability. The amount of antibody molecules conjugated with microspheres was determined by monitoring the difference in UV absorption at 280 nm of the Ab_2 solution before and after adsorption. The difference in the amount of Ab_2 before (30.00 $\mu g\,mL^{-1}$) and after adsorption (10.18 $\mu g\,mL^{-1}$) represents the amount of Ab_2 adsorbed on the surface of the hybrid material. The adsorbed amount of Ab_2 was estimated to be 19.82 $\mu g\,mL^{-1}$ in the stock dispersion.

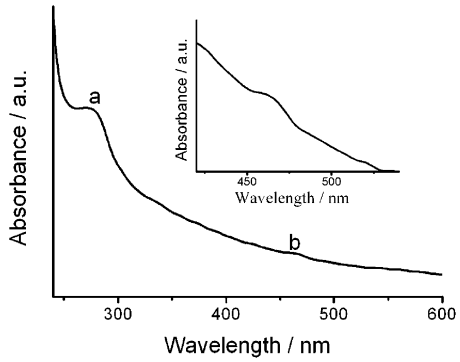

Figure 4. UV/Vis absorption of Fe_3O_4@$MnCO_3$@PEs-CdTe-Ab_2 bioconjugate. Inset: magnification of CdTe peaks in the absorption spectrum of Fe_3O_4@$MnCO_3$@PEs-CdTe-Ab_2.

Preparation of polydopamine (PDA) surface for immobilizing AFP capture antibodies (Ab_1): A PDA film was used to immobilize Ab_1 by a facile approach.[45] Dopamine, a biomolecule that contains catechol and amino functional groups, and is also found in high concentration in mussel adhesive proteins, polymerizes at alkaline pH to form thin ad-

 © 2011 Wiley-VCH Verlag GmbH & Co. KGaA, Weinheim

herent PDA films that exhibit latent reactivity toward amino and thiol groups. The reactivity of the polydopamine film was exploited to covalently immobilize proteins on the surface through a reaction between nucleophiles and the polydopamine surface. Atomic force microscopy (AFM) was employed to characterize PDA films and Ab_1-immobilized PDA. As shown in Figure 5A, the PDA film on a glass surface is complete, homogenous, and well ordered. Figure 5B shows that the Ab_1 is coated on the PDA film after the reaction between Ab_1 and PDA. Distinctive difference in the topography between in Figure 5A and B can be observed before and after the binding of Ab_1, which indicates that Ab_1 is effectively bound to the PDA surface.

Immunosensor fabrication: The Fe_3O_4@$MnCO_3$@PEs-CdTe microspheres have advantages such as excellent superparamagnetic and fluorescence properties, as well as outstanding biocompatibility, which make them promising for bioapplications. AFP is a major plasma protein produced by the yolk sac and the liver. AFP expression is often associated with hepatoma and teratoma and has been widely used as a diagnostic biomarker for hepatocellular carcinoma.[46] We used AFP as a model cancer biomarker to demonstrate application of Fe_3O_4@$MnCO_3$@PEs-CdTe microspheres conjugated with Ab_2 as a biolabel. The fabrication process of the immunosensor is depicted in Scheme 1b. Briefly, after the substrate surface was coated with PDA film, Ab_1 was immobilized on the substrate. Then, the AFP antigen was added to react with Ab_1. Next, the Fe_3O_4@$MnCO_3$@PEs-CdTe-Ab_2 bioconjugates were captured on the surface by antigen–antibody reaction.

Fluorescence imaging: To demonstrate the practicality of the proposed system, the multifunctional particles were used as a probe for immunosensing events on a glass surface, monitored by fluorescence microscopy (Figure 6). In the control experiment, no fluorescence was observed (Figure 6A). In the presence of 1.0 ng mL^{-1} AFP (Figure 6B), a strong green fluorescence was observed at the immunoreaction sites, indicating the potential of the probe for photoluminescence detection.

Stripping voltammetric analysis: By using the Fe_3O_4@$MnCO_3$@PEs-CdTe-Ab_2 bioconjugates as labels, a promising immunosensor for the electrochemical detection of AFP was developed. Square-wave stripping voltammetry (SWV) is a very sensitive technique for metal trace analysis and has very low limits of detection with a preconcentration feature.[47] The electrochemical signal was tested by determining the cadmium ions released from the biolabels by SWV. The SWV response is strongly influenced by the assay conditions. Therefore, the concentration of Ab_1, incubation temperature, incubation time, and the concentration of bioconjugates were investigated (Figure S4, Supporting Information). As the Ab_1 concentration increased from 10 to 50 μg mL^{-1}, the peak current increased and tended toward a stable signal at 30 μg mL^{-1}. As a result, a concentration of 30 μg mL^{-1} Ab_1 was selected for the further studies. The response increases with incubation time between 10 and 30 min and then levels off above 30 min. This indicates that the interaction of antigen with antibody had reached equilibrium after 30 min, and hence an incubation time of 30 min was selected in the experiments. The maximum response occurs at a reaction temperature of 37 °C, which might be attributed to denaturing of proteins at higher temperature and low immunoreaction efficiency at lower temperature. The response increased with concentration and reached a platform at 50 μg mL^{-1} of bioconjugate.

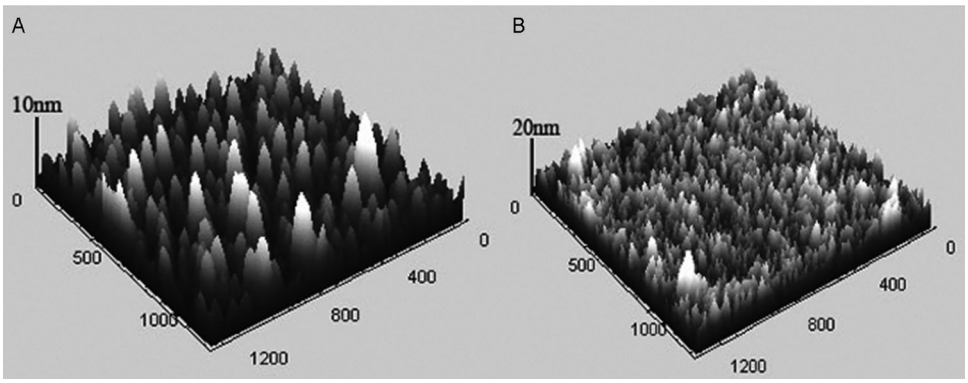

Figure 5. AFM images of A) PDA-coated glass substrate. B) Immobilization of Ab_1 on PDA films.

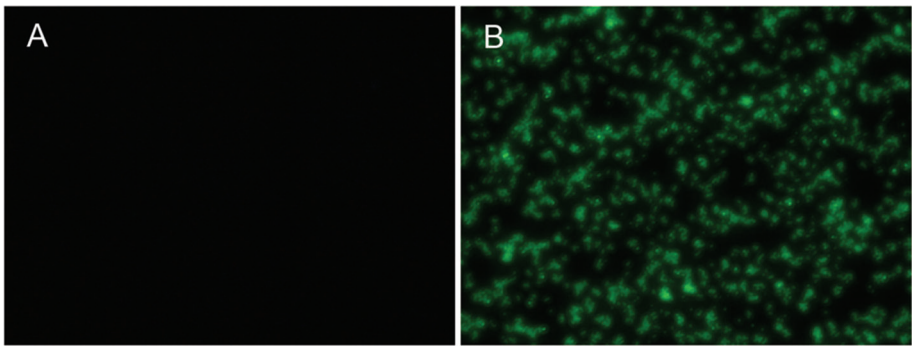

Figure 6. Fluorescence microscopic image of Fe_3O_4@$MnCO_3$@PEs-CdTe-Ab_2 bioconjugates as labels for sandwich immunoreaction. A) Control experiment without AFP antigen. B) With AFP concentration of 1.0 ng mL^{-1}.

© 2011 Wiley-VCH Verlag GmbH & Co. KGaA, Weinheim

Figure 7A displays typical SWV curves of the immunoassay with different concentrations of AFP. The peak current increases linearly with increasing logarithm of the AFP concentration over the range of 0.001–10 ng mL^{-1} (Figure 7B). The linear regression equation is $I/\mu A = 10.54 + 2438 \lg(C_{AFP}/ng\,mL^{-1})$, with a linear regression coefficient of 0.996. The detection limit ($S/N = 3$) was estimated to be 0.3 pg mL^{-1}.

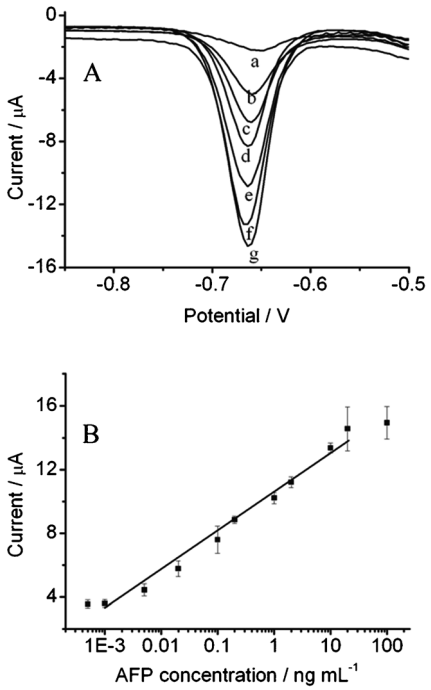

Figure 7. A) Typical SWV curves of electrochemical immunoassay with AFP concentration of 0, 0.001, 0.01, 0.1, 1.0, 2.0, and 10 ng mL^{-1}(a–g, respectively). B) Resulting calibration curve of AFP plotted on a semi-log scale.

Specificity is an important criterion for any analytical tool. Other proteins such as tumor necrosis factor-alpha (TNF-α), immunoglobulin G (IgG), carcinoembryonic antigen (CEA), and human interlekin-6 (IL-6) were used to evaluate the selectivity of the immunoassay. The currents obtained for each interfering substance at a concentration of 10 ng mL^{-1} in the presence of 1.0 ng mL^{-1} AFP were used as an indicator for the assay selectivity in comparison with the AFP alone (Table 1). The ratio of currents for AFP alone and a mixture containing each interfering substance are 0.97, 1.02, 1.05, and 0.95, respectively, that is, no interference is observed. Immunoassay reproducibility was estimated by assaying one AFP level for five replicate measurements with relative standard deviations (RSD) of 6.0%. The storage stability of the Fe_3O_4@$MnCO_3$@PEs-CdTe-Ab_2 was investigated by comparison with the stripping signals after a sandwiched immunoreaction, which illustrated that 92.1% of the original reaction activity remained after two months of storage for dried biolabels at 4°C; when the biolabel was stored in PBS at 4°C, the stripping signals remained at about 98.3, 94.7, and 79.4% after two weeks, one month, and two months storage, respectively. This indicates good storage stability for the dried bioconjugates at 4°C.

Table 1. Possible interferences tested with the immunosensor.

Possible interference	Current ratio[a]
tumor necrosis factor-alpha (TNF-α)	0.97
immunoglobulin G (IgG)	1.02
carcinoembryonic antigen (CEA)	1.05
human interleukin-6 (IL-6)	0.95

[a] Ratio of currents for a mixture that contains 10 ng mL^{-1} of interfering substance and 1.0 ng mL^{-1} of AFP compared with that for 1.0 ng mL^{-1} of AFP.

Clinical applications in human serum: The feasibility of the immunoassay for clinical applications was investigated by analyzing real samples, in comparison with the ELISA method. The serum samples were diluted with PBS of pH 7.4. Table 2 describes the correlation between the partial results obtained by the proposed immunoassay and the ELISA method. No significant difference is observed between the results given by the two methods, that is, the proposed immunoassay can be satisfactorily applied to clinical determination of AFP levels in human plasma.

Table 2. Assay results of clinical serum samples for the proposed and ELISA methods.

Serum sample	Proposed method[a] [pg mL^{-1}]	ELISA[a] [pg mL^{-1}]	Relative deviation [%]
1	266	269	−1.1
2	1456	1399	4.1
3	1870	1921	2.7
4	234	232	0.9
5	81.9	83.4	−1.8

[a] Average value of three successive determinations.

Conclusion

Novel multifunctional $MnCO_3$ microspheres with superparamagnetic and fluorescent properties were synthesized through a simple route including a co-precipitation reaction and layer-by-layer technique. The rough surface of the Fe_3O_4@$MnCO_3$ microspheres offers an ideal template for QD loading. In addition, the polyelectrolyte layers also contribute to formation of a uniform distribution of CdTe QDs on the microspheres. The multifunctional $MnCO_3$ microspheres have advantages, such as superparamagnetism, outstanding fluorescence, and good solubility in water, and offer an optimized microenvironment for protein immobilization to fabricate Fe_3O_4@$MnCO_3$@PEs-CdTe-Ab_2 architecture. A promising and versatile platform was developed for fluorescence imaging and electrochemical detection of a cancer biomarker. The multifunctional $MnCO_3$ microspheres

 © 2011 Wiley-VCH Verlag GmbH & Co. KGaA, Weinheim

are expected to find other potential applications, such as drug delivery and diagnostics.

Experimental Section

Chemicals: α-Fetoprotein (AFP), monoclonal capture (Ab_1), and signal anti-AFP antibodies (Ab_2) were purchased from Boson Biotechnology Co. Ltd. Poly(sodium 4-styrenesulfonate) (PSS, $M=70000$), poly(allylamine hydrochloride) (PAH, $M=15000$), 3-mercaptopropionic acid (MPA), bovine serum albumin (BSA), 1-ethyl-3-(3-dimethylaminopropyl) carbodiimide hydrochloride (EDC), *N*-hydroxysuccinimide (NHS), dopamine (DA), and Tween 20 were obtained from Aldrich Chemical Co. Phosphate buffer solution (PBS) with various pH was prepared by mixing stock solutions of NaH_2PO_4 and Na_2HPO_4, and then adjusting the pH with 0.1 M NaOH and H_3PO_4. All of other chemicals were of analytical grade. Doubly distilled water was used throughout the experiments. The clinical serum samples were from Nanjing Gulou Hospital.

Synthesis of Fe_3O_4@$MnCO_3$ microspheres: Fe_3O_4 nanoparticles (50 mg) were added to $MnSO_4$ (100 mL, 0.016 M) in glycerol/water (1/1, v/v) and stirred for 30 min. NH_4HCO_3 (100 mL, 0.16 M) in glycerol/water (1/1, v/v) was then added and the mixture stirred for 1 h at 50 °C. Finally, the precipitate was centrifuged and washed with water three times.

Assembly of CdTe QDs on Fe_3O_4@$MnCO_3$ microspheres: Fe_3O_4@$MnCO_3$ microspheres (10 mg) were suspended in PSS or PAH solution (2 mL, 2.0 mg mL^{-1}) for 10 min, and excess polyelectrolyte was removed by magnetic separation/washing in water. Thus, Fe_3O_4@$MnCO_3$@PEs microspheres were obtained. The water-soluble CdTe QDs were prepared by our previous reported method.[16] The Fe_3O_4@$MnCO_3$@PEs microspheres were dispersed in a CdTe QDs solution (2 mL) and sonicated for 20 min. After magnetic separation, the Fe_3O_4@$MnCO_3$@PEs-CdTe hybrid was obtained, and the supernatant was used for the analysis of the loading. The composites were further washed with water three times.

Fabrication of Fe_3O_4@$MnCO_3$@PEs-CdTe-Ab_2 bioconjugates: 1 mL of resulting hybrid was mixed with Ab_2 solution (0.2 mL, 60 mg mL^{-1}) followed by addition of EDC (100 μL, 20 mg mL^{-1}) and NHS solution (100 μL, 10 mg mL^{-1}). After incubation for 2 h and washing with water, the bioconjugates were redispersed in PBS (10 mM, 1 mL) and stored at 4 °C for subsequent use.

Polydopamine (PDA) surface for immobilization of Ab_1: A glass substrate (GS) was immersed in an aqueous DA solution (2 mg mL^{-1}) in Tris buffer (10 mM, pH 8.5) for 24 h at room temperature and then washed three times. All the resulting glass substrates were stored at 4 °C when not in use.

Sandwich immunoreaction based on Fe_3O_4@$MnCO_3$@PEs-CdTe-Ab_2 labels: The PDA-coated GS (GS/PDA) was immersed in Ab_1 solution (40 μL, 40 mg mL^{-1}, pH 7.4) for 12 h at 4 °C. After washing with PBST, the Ab_1 immobilized GS was blocked with blocking solution (PBS containing 0.2% BSA) for 30 min at room temperature and washed with PBST. Then, GS/PDA/Ab_1 was incubated with AFP solution (40 μL) for 30 min at 37 °C. After incubation in Fe_3O_4@$MnCO_3$@PEs-CdTe-Ab_2 bioconjugates solution (40 μL, 50 μg mL^{-1}) for 30 min, the substrate was washed with PBST to remove nonspecifically bound conjugates.

Stripping voltammetric analysis: 100 μL of HNO_3 (0.1 M) solution was employed to release cadmium ions from the captured biolabels. The resulting solution was mixed with HOAc/NaOAc buffer (1.9 mL, 0.2 M, pH 4.6) to perform anodic stripping voltammetric detection with a mercury film modified glassy carbon electrode. The working electrode was prepared by deposition at −1.0 V for 3 min and scanning from −0.9 to −0.2 V in Hg^{2+} solution (40 μg mL^{-1}) in 0.2 M HOAc/NaOAc buffer (pH 4.6) under N_2 atmosphere. Anodic stripping detection was carried out by electrodepositing cadmium at −1.1 V for 4 min and then stripping from −0.9 V to −0.2 V under N_2 atmosphere with a square-wave voltammetric waveform, with 4 mV potential step, 15 Hz frequency, and amplitude of 25 mV.

Apparatus and characterization: The morphologies of as-prepared materials were observed by TEM (JEOL JEM-200CX) and SEM (LEO153VP). A SQUID magnetometer (Quantum Design) was used for magnetic measurements at 300 K. UV/Vis spectra were recorded on a Shimadzu UV-3600 spectrophotometer at room temperature. Zeta potentials were measured with a PALS Zeta Potential Analyzer Ver. 3.43 (Brookhaven Instruments Corp.). The fluorescence spectra were recorded on a RF-5301 PC spectrofluorophotometer (Shimadzu). Confocal micrographs were taken with a Leica TCS-SL confocal scanning system mounted to a Leica Aristoplan and equipped with a 40× oil-immersion objective with numerical aperture of 1.25. All AFM experiments were performed on SPA-300 HV with a SPI 3800 controller (Seiko) in tapping mode. Electrochemical experiments were performed with a CHI660 workstation (Shanghai Chenhua, Shanghai, China). All differential pulse voltammetric measurements were carried out by using a conventional three-electrode system with a glassy carbon working electrode, saturated calomel electrode, and a platinum counterelectrode.

Acknowledgements

We greatly appreciate the support of the National Natural Science Foundation of China (20821063 and 21075061) and the Natural Science Foundation of Jiangsu Province (BK2010363). This work is also supported by National Basic Research Program of China (2011CB933502) and the Fundamental Research Funds for the Central Universities (1112020504).

[1] Z. H. Nie, A. Petukhova, E. Kumacheva, *Nat. Nanotechnol.* **2010**, *5*, 15–25.
[2] T. K. Sau, A. L. Rogach, F. Jackel, T. A. Klar, J. Feldmann, *Adv. Mater.* **2010**, *22*, 1805–1825.
[3] L. Zhang, S. Z. Qiao, Y. G. Jin, H. G. Yang, S. Budihartono, F. Stahr, Z. F. Yan, X. L. Wang, Z. P. Hao, G. Q. Lu, *Adv. Funct. Mater.* **2008**, *18*, 3203–3212.
[4] N. Insin, J. B. Tracy, H. Lee, J. P. Zimmer, R. M. Westervelt, M. G. Bawendi, *ACS Nano* **2008**, *2*, 197–202.
[5] N. Modak, A. Datta, R. Ganguly, *Microfluid. Nanofluid.* **2009**, *6*, 647–660.
[6] S. P. Chen, X. D. Yu, J. J. Xu, H. Y. Chen, *Analyst* **2010**, *135*, 2979–2986.
[7] L. Thazhe, A. Shereef, S. Shukla, C. P. Reshmi, M. R. Varma, K. G. Suresh, K. Patil, K. G. Warrier, *J. Am. Ceram. Soc.* **2010**, *93*, 3642–3650.
[8] C. Wang, S. Y. Tao, W. Wei, C. G. Meng, F. Y. Liu, M. Han, *J. Mater. Chem.* **2010**, *20*, 4635–4641.
[9] M. Bruchez, Jr., M. Moronne, P. Gin, S. Weiss, A. P. Alivisatos, *Science* **1998**, *281*, 2013–2016.
[10] R. Freeman, R. Gill, I. Shweky, M. Kotler, U. Banin, I. Willner, *Angew. Chem.* **2009**, *121*, 315–319; *Angew. Chem. Int. Ed.* **2009**, *48*, 309–313.
[11] Z. H. Li, Y. Wang, J. Wang, Z. W. Tang, J. G. Pounds, Y. H. Lin, *Anal. Chem.* **2010**, *82*, 7008–7014.
[12] X. A. Liu, L. X. Cheng, J. P. Lei, H. Liu, H. X. Ju, *Chem. Eur. J.* **2010**, *16*, 10764–10770.
[13] D. Geißler, L. J. Charbonnière, R. F. Ziessel, N. G. Butlin, H. G. Löhmannsröben, N. Hildebrandt, *Angew. Chem.* **2010**, *122*, 1438–1443; *Angew. Chem. Int. Ed.* **2010**, *49*, 1396–1401.
[14] X. Michalet, F. F. Pinaud, L. A. Bentolila, J. M. Tsay, S. Doose, J. J. Li, G. Sundaresan, A. M. Wu, S. S. Gambhir, S. Weiss, *Science* **2005**, *307*, 538–544.
[15] Y. Xing, J. H. Rao, *Cancer Biomarkers* **2008**, *4*, 307–319.
[16] R. Cui, H. C. Pan, J. J. Zhu, H. Y. Chen, *Anal. Chem.* **2007**, *79*, 8494–8501.
[17] K. Pinwattana, J. Wang, C. T. Lin, H. Wu, D. Du, Y. H. Lin, O. Chailapakul, *Biosens. Bioelectron.* **2010**, *26*, 1109–1113.
[18] H. Wang, J. Wang, C. Timchalk, Y. H. Lin, *Anal. Chem.* **2008**, *80*, 8477–8484.

 © 2011 Wiley-VCH Verlag GmbH & Co. KGaA, Weinheim

[19] J. Wang, G. D. Liu, H. Wu, Y. H. Lin, *Small* **2008**, *4*, 82–86.
[20] J. J. Zhou, H. P. Huang, J. Xuan, J. R. Zhang, J. J. Zhu, *Biosens. Bioelectron.* **2010**, *26*, 834–840.
[21] D. Y. Wang, A. L. Rogach, F. Caruso, *Nano Lett.* **2002**, *2*, 857–861.
[22] V. Salgueiriño-Maceira, M. A. Correa-Duarte, M. Spasova, L. M. Liz-Marzan, M. Farle, *Adv. Funct. Mater.* **2006**, *16*, 509–514.
[23] N. Gaponik, I. L. Radtchenko, G. B. Sukhorukov, A. L. Rogach, *Langmuir* **2004**, *20*, 1449–1452.
[24] N. Gaponik, I. L. Radtchenko, M. R. Gerstenberger, Y. A. Fedutik, G. B. Sukhorukov, A. L. Rogach, *Nano Lett.* **2003**, *3*, 369–372.
[25] S. T. Selvan, P. K. Patra, C. Y. Ang, J. Y. Ying, *Angew. Chem.* **2007**, *119*, 2500–2504; *Angew. Chem. Int. Ed.* **2007**, *46*, 2448–2452.
[26] D. K. Yi, S. T. Selvan, S. S. Lee, G. C. Papaefthymiou, D. Kundaliya, J. Y. Ying, *J. Am. Chem. Soc.* **2005**, *127*, 4990–4991.
[27] D. Muller-Schulte, T. Schmitz-Rode, P. Borm, *J. Magn. Magn. Mater.* **2005**, *293*, 135–143.
[28] P. Strobel, F. Thiery, C. Darie, O. Proux, A. Ibarra-Palos, M. Bacia, J. B. Soupart, *J. Mater. Chem.* **2005**, *15*, 4799–4808.
[29] M. J. Aragón, C. Perez-Vicente, J. L. Tirado, *Electrochem. Commun.* **2007**, *9*, 1744–1748.
[30] L. F. Cui, M. T. Niu, G. X. Chen, Y. S. Wang, *Mater. Lett.* **2009**, *63*, 2499–2502.
[31] J. B. Fei, Y. Cui, X. H. Yan, W. Qi, Y. Yang, K. W. Wang, Q. He, J. B. Li, *Adv. Mater.* **2008**, *20*, 452–456.
[32] L. X. Yang, Y. J. Zhu, H. Tong, W. W. Wang, *Ultrason. Sonochem.* **2007**, *14*, 259–265.
[33] W. Z. Wang, L. Ao, *Cryst. Growth Des.* **2008**, *8*, 358–362.
[34] L. L. del Mercato, P. Rivera-Gil, A. Z. Abbasi, M. Ochs, C. Ganas, I. Zins, C. Sonnichsen, W. J. Parak, *Nanoscale* **2010**, *2*, 458–467.
[35] H. G. Zhu, E. W. Stein, Z. H. Lu, Y. M. Lvov, M. J. McShane, *Chem. Mater.* **2005**, *17*, 2323–2328.
[36] B. G. De Geest, C. Dejugnat, M. Prevot, G. B. Sukhorukov, J. Demeester, S. C. De Smedt, *Adv. Funct. Mater.* **2007**, *17*, 531–537.
[37] W. Qi, A. H. Wang, Y. Yang, M. C. Du, M. N. Bouchu, P. Boullanger, J. B. Li, *J. Mater. Chem.* **2010**, *20*, 2121–2127.
[38] Y. Zhu, W. J. Tong, C. Y. Gao, H. Mohwald, *J. Mater. Chem.* **2008**, *18*, 1153–1158.
[39] Y. J. Wang, A. D. Price, F. Caruso, *J. Mater. Chem.* **2009**, *19*, 6451–6464.
[40] R. J. Zhang, D. M. Lu, Z. G. Lin, L. Li, W. R. Jin, H. Mohwald, *J. Mater. Chem.* **2009**, *19*, 1458–1463.
[41] S. Chinnayelka, M. J. McShane, *Anal Chem.* **2005**, *77*, 5501–5511.
[42] T. S. Corbitt, J. R. Sommer, S. Chemburu, K. Ogawa, L. K. Ista, G. P. Lopez, D. G. Whitten, K. S. Schanze, *ACS Appl. Mater. Interfaces* **2009**, *1*, 48–52.
[43] X. Jia, D. R. Chen, X. L. Jiao, S. M. Zhai, *Chem. Commun.* **2009**, 968–970.
[44] T. R. Sathe, A. Agrawal, S. M. Nie, *Anal. Chem.* **2006**, *78*, 5627–5632.
[45] H. Lee, J. Rho, P. B. Messersmith, *Adv. Mater.* **2009**, *21*, 431–434.
[46] Y. Tamura, S. Yamagiwa, Y. Aoki, S. Kurita, T. Suda, S. Ohkoshi, M. Nomoto, Y. Aoyagi, G. Niigata Liver Dis Study, *Dig. Dis. Sci.* **2009**, *54*, 2530–2537.
[47] G. D. Liu, H. Wu, J. Wang, Y. H. Lin, *Small* **2006**, *2*, 1139–1143.

Received: March 23, 2011
Revised: June 27, 2011
Published online: August 11, 2011

 © 2011 Wiley-VCH Verlag GmbH & Co. KGaA, Weinheim